Seventh International Conference on CFD in the Minerals and Process Industries
CSIRO, Melbourne, Australia
9-11 December 2009

MODELLING SUBMICRON AND MICRON PARTICLE DEPOSITION IN A HUMAN NASAL CAVITY

Kiao INTHAVONG[1], Kai ZHANG[1], Jiyuan TU[1]

[1] School of Aerospace, Mechanical and Manufacturing Engineering, RMIT University, PO Box 71, Bundoora Vic 3083, AUSTRALIA

ABSTRACT

The size of a particle determines the deposition efficiency, as well as its deposition site. In this paper, different modelling techniques are presented for submicron and micron particles in a human nasal cavity. In addition this paper highlights some deficiencies in the default models available in a commercially available CFD software.For submicron particles the default Fluent Brownian model and a User-Defined Brownian model were evaluated. It was found that the default Brownian model significantly underpredicted submicron particle deposition, while the User Defined Brownian model provided an improvement in the particle deposition. The default Fluent turbulent particle tracking is known to overpredict the deposition of low inertial particles. This was evaluated against a damping function applied in the near wall region to reduce the normal fluctuating velocity. The application of the damping function improved the deposition efficiency for the low inertial particles.

NOMENCLATURE

d	particle diameter
g	gravity
k	turbulent kinetic energy
k_B	Boltman Constant
p	pressure
Q	flow rate
u	velocity
u_i'	fluctuating velocity
ν	kinematic viscosity
ρ	density
μ	dynamic viscosity
λ	mean free path
Re	Reynolds number

INTRODUCTION

The sizes of inhalable airborne particles exist on multiscale levels. For instance smoke, airborne viruses, and fumes all exist on a submicron level, while nasal spray drug particles, pollen, and dust are on a micron level. The size of the particle determines the deposition efficiency, as well as its deposition site. It also governs the type of flight path a particle experiences in relation to the surrounding fluid flow. Submicron particles which become so small (nanoparticle range) that the fluid can no longer be considered a continuum, experience a diffusion flight path leading to a diffusional deposition. Micron particles are dominated by its inertial property which lead to inertial impaction upon sudden changes in the airflow streamlines. In the absence of a convective flow the particles settle due to gravity leading to deposition by gravitational sedimentation.

It is therefore clear that different particle sizes require different modelling needs. The simulation of nanoparticle deposition was performed by Zamankhan et al. (2006) under steady laminar conditions where diffusion was the dominant deposition mechanism for the smallest range of particles (1–30 nm). Shi et al. (2006) and Zhang et al. (2005) also simulated the transport and deposition of nanoparticles, d_p=1-2 nm and ultrafine particles, d_p =5 nm under a transient laminar flow in a representative human nasal cavity. Some issues have been raised by (Longest and Xi 2007b) in terms of the Fluent's (a commercial CFD software) Brownian model which will be explored further in this paper.

Micron particle deposition under a laminar flow has been simulated by a number of researchers (Schroeter et al. 2006; Tian et al. 2007). One challenging problem arising from micron particle deposition is the handling of the turbulent dispersion. In one-way coupled turbulent dispersion of particles, the isotropic turbulence assumption of RANS turbulence models becomes problematic in wall bounded flows such as the nasal cavity. The turbulent dispersion of particles is determined by the stochastic process through the Eddy Interaction Model (EIM). Within this model the fluctuating velocity components u_i' are taken from the local root mean square (RMS) velocity fluctuation by

$$\sqrt{\overline{u_i'^2}} = \sqrt{2k_g/3} \quad (1)$$

However the isotropic assumption (i.e. $u' = v' = w'$) leads to an overestimation of the normal fluctuating velocity component in the near wall region. This causes an overestimation of deposition for the smaller range of particles (<10μm) (Macinnes and Bracco 1992; Wang and James 1999; Zhang et al. 2004) due to the particle's shorter relaxation time. Improved models for the EIM model is proposed by Wang and James (1999), Matida et al. (2004), Dehbi (2008), and Tian and Ahmadi (2007). Another possibility is to use Large Eddy Simulations (LES) which is quite computationally expensive and requires a robust boundary conditions and high quality mesh set up, however LES models are quite difficult for complex geometries.

In this paper, modelling techniques to account for submicron and micron particles are discussed. The default Fluent Brownian model (Fluent-BM), along with a user-defined-function Brownian model (UDF-BM) under a laminar flow is evaluated to determine the validity of the models. For micron particles a different approach to

account for the turbulent dispersion is used here. The *k-ω* SST low-Re turbulence model is used to model the flow field while a slight modification to the EIM model is made to account for turbulent dispersion in the near wall region. Successful modelling of submicron and micron particles will allow more flexibility in simulations of gas-particle flows for inhalation toxicology, and drug delivery studies through the human respiratory system.

MODEL DESCRIPTION

Development of Computational Model

Three geometries are created for this study. The first two are a straight pipe and a 90-degreee bend pipe based on the analytic and experimental deposition data (Fig.1). For the human nasal cavity, CT scans provide the three-dimensional outline through the use of x-rays. Helical CT scans were used as the amount of time that the patient needs to lie down is reduced and therefore higher scan resolution can be achieved. A scan of the nasal cavity was obtained from a healthy 25 year old, Asian male, 170cm height, 75 kg mass. The CT scan was performed using a CTI Whole Body Scanner (General Electric).

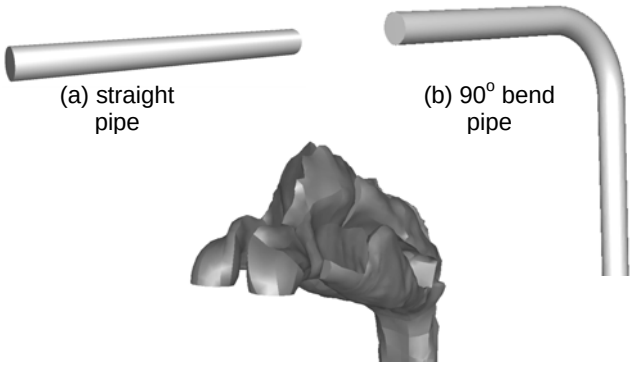

Fig.1 Reconstructed geometries of (a) straight pipe (b) 90° bend pipe (c) and a human nasal cavity

The scans acquired were of contiguous images (slices) of 1-5 mm thickness with voxel size of 0.625 x 0.625 x 1 mm. The field of view was 40-cm (FOV), with a power of 120 kV peak and 200 mA. The CFD model was created using Mimics and GAMBIT software. Additional details can be found in Inthavong et al. (2009) for the nasal cavity construction. Table 1 summarises the geometries and some key dimensions.

TABLE 1 Dimensions and details of the four geometries considered in this study

	Inlet Hydraulic Diameter (D_h)	Radius of curvature	Inlet Flow Rate (L/min)	Inlet Re number	Mesh size
Straight pipe	0.45 cm	-	1 10 60	322 3228 19370	750,000
90° bend pipe	0.46 cm	1.43 cm	1.052	305	550,000
Nasal cavity	1.0 cm	1.50 cm*	10 20	1452 2904	1.4 mil

*nostril-nasal valve bend

Fluid Flow Modelling

The geometries were inputted into the commercial CFD code, FLUENT 6.3.26, where the governing equations for fluid flow under steady-state conditions were modelled. Flow rates of 1, 10, and 60 L/min were used for the straight pipe and 90° bend pipe while a flow rate of 10 L/min was used for the nasal cavity and the lung airway. At 10L/min the flow regime in the respiratory airways has been determined as dominantly laminar (Hahn et al. 1993; Kelly et al. 2000; Swift and Proctor 1977; Zamankhan et al. 2006) and the quasi-steady assumption can be applied through the Womersley parameter and the Strouhal number (Wen et al. 2008). The steady-state continuity and momentum equations under Reynolds averaging can be found in Wilcox (1993). The equations were discretised with the QUICK scheme while the pressure-velocity coupling was resolved through the SIMPLE method.

Particle Flow Modelling

For a low volume fraction of dispersed phase (particles), the Lagrangian approach with one-way coupling is used, i.e. the airflow transports the particles, but the effect of particle movements on the flow is neglected. In this approach, the airflow field is first simulated, and then the trajectories of individual particles are tracked by integrating a force balance equation on the particle, which can be written as:

$$\frac{du_i^p}{dt} = F_D + F_g + F_B + F_S \tag{2}$$

F_g is the gravity term, which is defined as

$$F_g = \frac{g(\rho_p - \rho_g)}{\rho_p} \tag{3}$$

and ρ_p and ρ_g denotes the density of particle material and air, respectively. F_D is the drag force per unit particle mass taking the form of Stokes' drag law (Ounis et al. 1991) defined as,

$$F_D = \frac{18\mu}{d_p^2 \rho_p C_c}\left(u_i^g - u_i^p\right) \tag{4}$$

C_c is the Cunningham correction factor to Stokes' drag law, which can be calculated from,

$$C_c = 1 + \frac{2\lambda}{d_p}\left(1.257 + 0.4e^{-\left(1.1 d_p/2\lambda\right)}\right) \tag{5}$$

where λ is the mean free path of air, assumed to be 65 nm.

Submicron Particle Modelling

Amplitudes of the Brownian force components are of the form,

$$F_B = \zeta\sqrt{\frac{\pi S_0}{\Delta t}} \tag{6}$$

where ζ is a zero mean, unit variance independent Gaussian random numbers. Δt is the time-step for particle integration, and S_o is a spectral intensity function,

$$S_0 = \frac{216\nu k_B T}{\pi^2 \rho d_p^5 \left(\frac{\rho_p}{\rho}\right)^2 C_c} \tag{7}$$

which is directly related to the diffusion coefficient. The Brownian force expression can be re-arranged to highlight the diffusion coefficient as:

$$F_B = \frac{\zeta}{m_d}\sqrt{\frac{1}{\tilde{D}}\frac{2k_B{}^2 T^2}{\Delta t}} \tag{8}$$

where m_d is the mass of the particle, T is the absolute temperature of the fluid, v is the kinematic viscosity, k_B is the Boltzmann constant, and $\tilde{D}$ is the diffusion coefficient. Equation (8) is inputted into the user-defined-function option in Fluent and is referred to as (UDF-BM).

The UDF-BM is as an alternate model to the default Fluent-BM.

$$\tilde{D} = \frac{k_B T C_c}{3\pi\mu d_p} \tag{9}$$

F_s includes additional body forces such as the lift force and thermophoretic force given in Saffman (1965) and Talbot et al. (1980) respectively.

The Eulerian approach to modelling the nanoparticle diffusion involves a single mixture fluid with the nanoparticles treated as a chemical species. A scalar c, representing the concentration of the nanoparticles is applied to the transport equation as:

$$\frac{\partial(u_j c)}{\partial x_j} = \frac{\partial}{\partial x_j}\left[\left(\tilde{D} + \frac{\upsilon_T}{S}\right)\frac{\partial c}{\partial x_j}\right] \tag{10}$$

which neglects the effects of particle inertia. Particle rebounding from the surfaces was ignored and particle deposition was determined when the distance between the particle centre and a surface was less than or equal to the particle radius. The particle tracking is then terminated.

Turbulent Dispersion of Micron Particles

Turbulent dispersion of particles are handled by integrating the trajectory equations for individual droplets, using the instantaneous fluid velocity, $u^g_i + u_i'(t)$, along the particle path. Here, the discrete Eddy Interaction Model (EIM) is used where the fluctuating velocity components u_i' that prevail during the lifetime of the turbulent eddy are sampled by assuming that they obey a Gaussian probability distribution so that

$$u_i' = \zeta\sqrt{\overline{u_i'^2}} \tag{11}$$

ζ is a normally distributed random number and the remaining right-hand side is the local root mean square (RMS) velocity fluctuation can be obtained (assuming isotropy) by:

$$\sqrt{\overline{u_i'^2}} = \sqrt{2k_g/3} \tag{12}$$

The isotropy assumption becomes significant for human nasal cavity particle flows as the flow is at a low Reynolds number and the geometry is a wall bounded type flow. The isotropic assumption (i.e. $u' = v' = w'$) leads to an overestimation of the normal fluctuating velocity component, w' in the near wall region. This causes an overestimation of deposition for the smaller range of particles (<<10μm) (Macinnes and Bracco 1992; Wang and James 1999; Zhang et al. 2004). This overestimation at the near wall region increases in sensitivity for smaller particles that have a shorter relaxation time. In an earlier study by the authors (Inthavong et al. 2006), a combined mean flow (laminar) tracking and EIM tracking was used for low and high inertial particles respectively. An improved model for the random walk method is proposed by Wang and James (1999) and Matida et al. (2004) and is applied here as a near wall correction to account for the anisotropic behaviour of turbulence by damping the turbulent kinetic energy. The damping function is applied up to y+ of 30 and is given as:

$$k_{new} = [1 - \exp(-0.02y^+)]^2\, k_{simulated} \tag{13}$$

The number of droplets tracked was checked for statistical independence since the turbulent dispersion is modelled based on a stochastic process. Independence was achieved for 30,000 droplets since an increase of droplets to 50,000 droplets yielded a difference of 0.1% in the inhalation efficiency. To achieve the uniform droplet concentration assumption, droplets were released at the same velocity as the freestream. It is assumed that the droplets will not affect the fluid flow (one-way coupling) as the volume fraction of the droplets was relatively low (<10%). Other assumptions include: i) no droplet rebounding off the walls/surfaces; ii) no droplet coagulation in the droplet deposition process and iii) all droplets are spherical and non-deforming.

Boundary Conditions

In order to achieve a fully developed flow throughout the computational domain for the straight and 90° bend pipes, an additional separate pipe 5D in length with the same cross-section and mesh were simulated with periodic boundaries. When the flow reached a fully developed state the velocity profile of one cross-section of the separate periodic straight pipe model was used as the inflow condition at the inlet of the 90° bend pipe and the straight pipe. Boundary conditions for the particles were set up as a circular particle release entrained in the flow field. Particles were released from 0.01m from the inlet to prevent any spurious data exiting the inlet upon immediate release. In addition the radial distance a particle was located was at no less than 0.1mm away from the wall to eliminate any artificial immediate deposition on the walls.

RESULTS

Submicron particle Deposition

Deposition results for the two Browniam motion models (Fluent-BM and the UDF-BM) are first verified through deposition efficiencies in the straight pipe and 90° bend pipe before applying the models to the nasal cavity. The deposition efficiency from 1-100nm simulated in a straight pipe and a 90° bend pipe are shown in Fig.2.

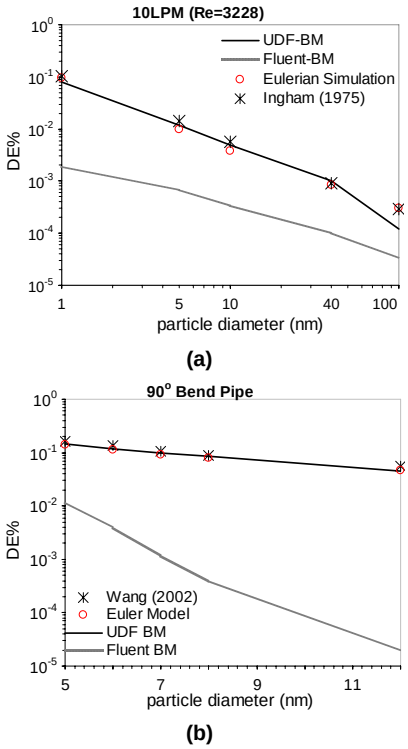

Fig.2 Deposition efficiency validation of the Fluent-BM and the UDF-BM model in a (a) straight pipe at 10LPM, and (b) 90° bend pipe.

The straight pipe was simulated at a flow rate of 10L/min while the bend pipe matched the flow conditions of Wang et al. (2002). For both cases, the Eulerian simulations capture the particle diffusion well. Some deviation from the empirical correlation of Ingham (1975) is found for particles approaching 100nm. The Eulerian approach models the concentration of the nanoparticles through the computational domain where the Brownian motion is accounted for through the diffusion coefficient $\tilde{D}$ as given in Eqn.(10). In this approach the effects of particle inertia is neglected and it was shown by Longest and Xi (2007a) that particle inertia on area-averaged deposition efficiency needed to be considered for particle Stokes numbers above 5×10^{-5}. For the straight pipe this corresponds only to the larger particles under investigation, e.g. 100nm particles at a flow rate of 10L/min.

Furthermore slip effects are not considered in the diffusion coefficient $\tilde{D}$ whereas it is inclusive within the drag force through the Cunningham slip correction, C_c applied onto the particles. The absence of the slip term becomes increasingly significant with decreasing particle size since the C_c is an inverse exponential function of the particle diameter d_p. The higher the slip, the weaker the coupling is between the particles and the fluid, leading to deviations from streamlines and increases in the residence times. Verification of the numerical results from the Fluent-BM indeed confirms the fallibility of the Brownian motion when implemented with through the default Fluent-BM. Large under-predictions are found for the Fluent-BM especially for 1nm particles in the straight pipe while for the bend pipe larger differences are found for 100nm. The UDF-BM results on the other hand, show improved results with the data matching the empirical correlation more closely.

Comparisons of the simulated results were made with the available experimental data reported by Cheng et al. (1996) for different nasal cavities. Here the solid line corresponds to the model prediction (Fig.3).

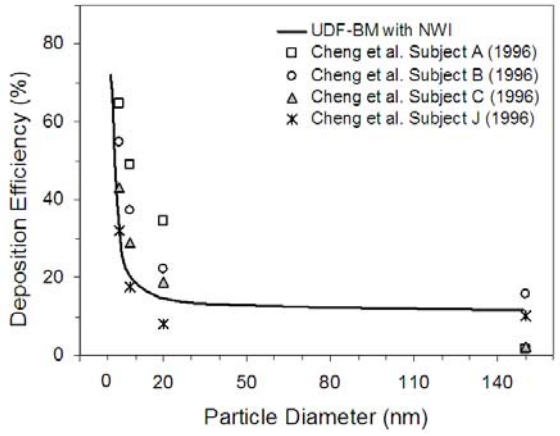

Fig.3 Deposition efficiency of 1nm-150nm particles in a human nasal cavity at a steady inhalation rate of 10L/min.

The deposition curve is high for very small nanoparticles and the particle diameter range in which the deposition drops from 72% to 18% is between 1nm-10nm. From 10nm-150nm however, there is only a small change in the deposition curve from 18%-15%. This deposition curve profile is characteristic of the Brownian diffusion, where the particles are so small that the fluid may no longer be considered continuous. The trajectory of the nanoparticle is then caused by the collision of the air molecules and concentration gradients to produce the random motion. The diffusion coefficient which is the main contributor to the Brownian motion is proportional to the slip correction, C_c and inversely proportional to particle size which explains the high gradient found in the deposition curve for particles in the range of 1nm-10nm.

Local deposition patterns for a 1nm particle are shown in Fig.4. A particle was deemed deposited if its trajectory impacted onto the wall surfaces, otherwise the particle escaped through the outlet. The deposition pattern is distributed evenly through the nasal cavity where the diffusion of 1nm particles disperses the particles in all directions. Few particles are able to reach the wider meatus region, and instead rather the particles remain close to the nasal septum wall (inner regions). High local concentration is found at the upper regions of the cavity with a higher distribution of deposition within that one area. In general the deposition pattern is spread out through the nasal cavity well. This has interesting applications for drug delivery where traditional nasal sprays are producing micron sized droplets that are prone to inertial deposition. This deposition mechanism leads to high inertial impaction (up to 100% for the mean atomised particle droplet of 50μm) in the anterior region of the nasal cavity (Inthavong et al. 2006; Inthavong et al. 2008). However for high drug efficacy, the delivery of the drug droplets needs to be deposited in the middle regions of the nasal cavity, where the highly vascularised walls exist. Smaller particles such as 1μm were found to be less affected by inertial properties, which allowed it to bypass the anterior region of the nasal cavity. However because of the particles ability to follow the streamlines more readily, the particles were less likely to deposit in any region of the nasal cavity and would bypass it completely, leading to the undesired effects of lung deposition. Delivery of nanoparticles especially 1nm-5nm particles therefore, can provide improved deposition in the middle regions whilst minimising deep lung deposition.

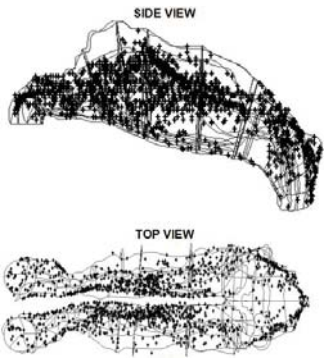

Fig.4 Deposition patterns of 1nm particles under a flow rate of 10L/min in a human nasal cavity

Micron particle Deposition

The left side of the nasal cavity was used for the particle deposition efficiency for micron particles under a flow rate of 20L/min passing through the nostril inlet. This corresponds to a Re number of 2904. Tracking of the particle dispersion was considered through the EIM-model, with and without the near wall damping of the turbulent kinetic energy (TKE), and are labelled as Modified TKE Simulation and EIM Simulation

respectively. Simulations of the particle deposition in the left nasal cavity (**Fig.5**) show an overprediction of low inertial particles. This is caused by the isotropic turbulence assumption of the EIM model as discussed earlier. Here the overprediction of the normal fluctuating velocity *w'* becomes significant for inertial impaction of smaller particles which have a shorter relaxation time, leading to particles directed towards the walls more readily.

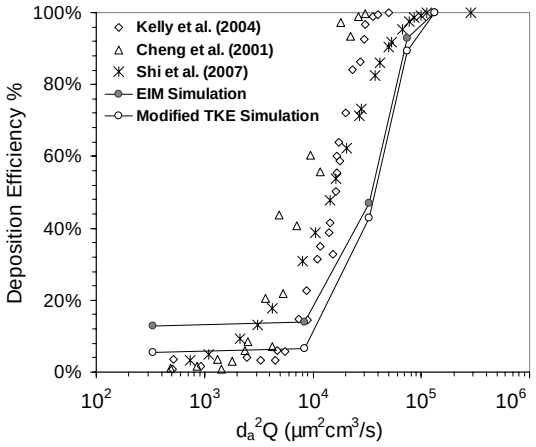

Fig.5 Inertial deposition efficiency for micron particles in the left cavity side of a human nasal cavity

A modification to the model by dampening the turbulent kinetic energy allows the normal fluctuating velocity to be reduced closer to its correct value. This effect reduces the particle deposition significantly for smaller particles. The simulated deposition curves are found to the right in comparison with the experimental data. This means that the larger inertial particles are underpredicted by both models. This discrepancy can be attributed to two modelling issues which are not investigated in this paper.

Firstly the geometries of the nasal cavities are different which may possess less deposition for wider airways (Häußermann et al. 2001). Furthermore, Kelly et al. (2004) points out that differences in comparison of particle inertial deposition with different nasal cavity models can be explained by inertial impaction considerations. For $d^2_{ae}\,Q$ values less than 2000 μm^{2}cm^3/s particles have a short relaxation time, which allows the particles to adjust to flow streamlines and hence the effect of different geometries is less significant. Accordingly the comparison between the deposition curve of the CFD simulation and the experimental data is fairly similar at this lower range after the TKE modification. As the value of $d^2_{ae}\,Q$ increases the particles relaxation time increases and the particles are more likely to continue a linear trajectory that deviates from a curving streamline. The differences in geometries that cause curvatures in streamlines are therefore more significant for larger inertial particles and greater deviation between different geometries is reasonable.

Secondly modelling issues that make the simulation more complex include a quasi-wall roughness model (Shi et al. 2007) implemented through an additional diffusion term in a laminar momentum equation allowed the deposition curve to be shifted to the left to match the experimental data more closely. Also a particle entering any part of a cell takes u_i^g from the cell centre. For cells adjacent to the wall boundaries, the velocity profile should approach zero at the wall rather than be uniform throughout the cell. Therefore a near wall interpolation scheme (Pepper and Heinrich 1992) which considers the influence of the zero velocity at the wall boundary as well as the convective fluxes of the surrounding cells can be applied.

Individual particle deposition locations are shown in **Fig.6** which highlights the different regions of inertial impaction and reduction in deposition when the Modified TKE Simulation model is applied. For the EIM model, high deposition is found in the anterior region of the nasal cavity.

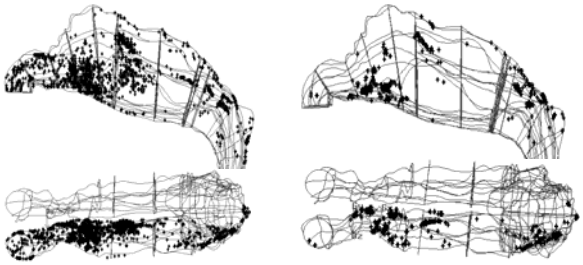

Fig.6 Deposition pattern for 1μm particle under the (a) EIM Simulation and (b) Modified TKE Simulation.

When the TKE is modified the deposition efficiency drops and the local regions of deposition is now smaller and mainly around the beginning of the main nasal passage in the middle region as well as at the nasopharynx region. Comparison of the deposition patterns in Figure 6a and b between the two models suggest that the damping of the TKE is most significant in the regions that exhibited a change from initial deposition to no deposition after the modification. This can be confirmed by investigating the TKE in the near wall region. Wall contours of the TKE (**Fig.7**) show that maximal fluctuating velocities will occur in the anterior regions of the nasal cavity, where the flow experiences a lot of flow disturbances such as the converging-diverging geometry of the nasal valve region. The damping function reduces the TKE sufficiently in the anterior region of the nasal cavity which reduces the deposition in this region.

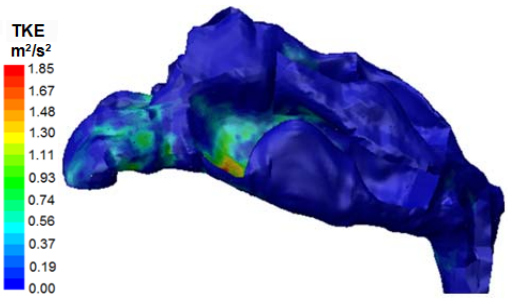

Fig.7 Contours of the TKE under the EIM simulation.

CONCLUSION

Two default models available in the commercial CFD software Fluent, are evaluated in order to simulate submicron and micron particles in a human nasal cavity. Although the models are applied to a human nasal cavity, the deficiencies of the models are generic and applicable

for similar flow conditions. The default Brownian model was found to be deficient for capturing the diffusion transport of submicron particles. This led to lower than expected dispersion of the particles and an underprediction of particle deposition. By applying a User-Defined Brownian model the deposition efficiency was improved. For micron particles the default EIM found in Fluent for turbulent particle tracking is known to overpredict the deposition of low inertial particles. This was evaluated against a damping function applied in the near wall region to reduce the normal fluctuating velocity. The application of the damping function improved the deposition efficiency for the low inertial particles. This paper highlights some shortcomings of available default models in commercial CFD software and provides one sample solution to rectify the shortcomings.

ACKNOWLEDGEMENTS

The financial support provided by the Australian Research Council (project ID LP0989452) and by RMIT University Emerging Research Grant are gratefully acknowledged.

REFERENCES

CHENG, K.H., CHENG, Y.S., YEH, H.C., GUILMETTE, A., SIMPSON, S.Q., YANG, Y.H., SWIFT, D.L. (1996) In-vivo measurements of nasal airway dimensions and ultrafine aerosol deposition in the human nasal and oral airways. *J. Aerosol Sci.* **27**, 785-801.

CHENG, Y.S., HOLMES, T.D., GAO, J., GUILMETTE, R.A., LI, S., SURAKITBANHARN, Y., ROWLINGS, C. (2001) Characterization of nasal spray pumps and deposition pattern in a replica of the human nasal airway. *J. Aerosol Med.* **14**, 267-280.

DEHBI, A. (2008) A CFD model for particle dispersion in turbulent boundary layer flows. *Nuclear Engineering and Design* **38**, 707-715.

HAHN, I., SCHERER, P.W., MOZELL, M.M. (1993) Velocity profiles measured for airflow through a large-scale model of the human nasal cavity. *J Appl. Physiol.* **75**, 2273-2287.

HÄUßERMANN, S., BAILEY, A.G., BAILEY, M.R., ETHERINGTON, G., YOUNGMAN, M.J. (2001) The influence of breathing patterns on particle deposition in a nasal replicate cast. *J. Aerosol Sci.* **33**, 923-933.

INGHAM, D.B. (1975) Diffusion of Aerosols from a Stream Flowing Through a Cylindrical Tube. *J. Aerosol Sci* **6**, 125-132.

INTHAVONG, K., TIAN, Z.F., LI, H.F., TU, J.Y., YANG, W., XUE, C.L., LI, C.G. (2006) A numerical study of spray particle deposition in a human nasal cavity. *Aerosol Science Technology* **40**.

INTHAVONG, K., TIAN, Z.F., TU, J.Y., YANG, W., XUE, C. (2008) Optimising nasal spray parameters for efficient drug delivery using computational fluid dynamics. *Computers in Biology and Medicine* **38**, 713-726.

INTHAVONG, K., WEN, J., TU, J.Y., TIAN, Z.F. (2009) From CT Scans to CFD Modelling – Fluid and Heat Transfer in a Realistic Human Nasal Cavity. *Engineering Applications of Computational Fluid Mechanics*.

KELLY, J.T., PRASAD, A.K., WEXLER, A.S. (2000) Detailed flow patterns in the nasal cavity. *J Appl. Physiol.* **89**, 323-337.

LONGEST, P.W., XI, J. (2007a) Computational investigation of particle inertia effects on submicron aerosol deposition in the respiratory tract. *Journal of Aerosol Science* **38**, 111-130.

LONGEST, P.W., XI, J. (2007b) Effectiveness of direct Lagrangian tracking models for simulating nanoparticle deposition in the upper airways. *Aerosol Science and Technology* **41**, 380-397.

MACINNES, J.M., BRACCO, F.V. (1992) Stochastic particle dispersion modeling and the tracer particle limit. *Physics of Fluids A* **4**, 2809-23.

MATIDA, E.A., FINLAY, W.H., LANGE, C.F., GRGIC, B. (2004) Improved numerical simulation fo aerosol deposition in an idealized mouth-throat. *J Aerosol Sci* **35**, 1-19.

OUNIS, H., AHMADI, G., J.B., M. (1991) Brownian diffusion of submicrometer particles in the viscous sublayer. *J. Colloid and Interface Science* **143**, 266-277.

PEPPER, D.W., HEINRICH, J.C. (1992) 'The Finite Element Method: Basic Concepts and Applications.' (Taylor and Francis: Bristol)

SAFFMAN, P.G. (1965) The lift on a small sphere in a slow shear flow. *J. Fluid Mech.* **22**, 385-400.

SCHROETER, J.D., KIMBELL, J.S., ASGHARIAN, B. (2006) Analysis of particle deposition in the turbinate and olfactory regions using a human nasal computational fluid dynamics model. *J. Aerosol Med.* **19**, 301-313.

SHI, H.W., KLEINSTREUER, C., ZHANG, Z. (2007) Modeling of inertial particle transport and deposition in human nasal cavities with wall roughness. *J. Aerosol Sci.* **38**, 398-419.

SHI, H.W., C. Kleinstreuer, ZHANG. Z. (2006). Laminar airflow and nanoparticle or vapor deposition in a human nasal cavity model. *J. Biomech. Eng*. **128**: 697-706.

SWIFT, D.L., PROCTOR, D.F. (1977) Access of air to the respiratory tract. In 'Respiratory Defence Mechanisms'. (Eds JD Brain, DF Proctor and LM Reid) pp. 63-93. (Marcel Dekker: New York, NY)

TALBOT, L., CHENG, R.K., SCHEFER, R.W., WILLIS, D.R. (1980) Thermophoresis of particles in a heated boundary layer. *J. Fluid Mech* **101**, 737-758.

TIAN, L., AHMADI, G. (2007) Particle deposition in turbulent duct flow- Comparison of different model predictions
J Aerosol Sci **38**, 377-397.

TIAN, Z.F., INTHAVONG, K., TU, J.Y. (2007) Deposition of inhaled wood dust in the nasal cavity. *Inhal. Toxicol.* **19**, 1155-1165.

WANG, J., FLAGAN, R.C., SEINFELD, J.H. (2002) Diffusional losses in particle sampling systems containing bends and elbows. *Journal of Aerosol Science* **33**, 843-857.

WANG, Y., JAMES, P.W. (1999) On the effect of anisotropy on the turbulent dispersion and deposition of small particles. *Int. J. of Multiphase Flows* **25**, 551-558.

WEN, J., INTHAVONG, K., TU, J.Y., WANG, S. (2008) Numerical simulations for detailed airflow dynamics in a human nasal cavity. *Respiratory Physiology & Neurobiology* **161**, 125-135.

WILCOX, D. (1993) 'Turbulence Modeling for CFD.' (DCW Industries, Inc.: 5354 Palm Drive, La Canada, California 91011)

ZAMANKHAN, P., AHMADI, G., WANG, Z., HOPKE, P.H., CHENG, Y.S., SU, W.C., LEONARD, D. (2006) Airflow and deposition of nanoparticles in a human nasal cavity. *Aerosol Sci. Technol.* **40**, 463-476.

ZHANG. Z., KLEINSTREUER. C., DONOHUE. J.F,. KIM. C.S. (2005) Comparison of micro- and nano-size particle depositions in a human upper airway model. *J Aerosol Sci* **36**, 211-33

ZHANG, Y., FINLAY, W.H., MATIDA, E.A. (2004) Particle deposition measurements and numerical simulation in a highly idealized mouth-throat. *J. Aerosol Sci.* **35**.

